water

MDPI

Article

Na-Kenyaite as Efficient Basic Blue-41 Dye Removal: Synthesis and Regeneration Studies

Osama Y. Al-Madanat [1,*], Saheed A. Popoola [2], Hmoud Al Dmour [3], Rawan Al-Faze [4] and Fethi Kooli [2,*]

[1] Chemistry Department, Faculty of Science, Mutah University, Karak 61710, Jordan
[2] Chemistry Department, Faculty of Science, Islamic University of Madinah, Madinah 42351, Saudi Arabia; abiodun@iu.edu.sa
[3] Physical Department, Faculty of Science, Mutah University, Karak 61710, Jordan; hmoud79@mutah.edu.jo
[4] Department of Chemistry, Faculty of Science, Taibah University, Medina 30002, Saudi Arabia
* Correspondence: madanat@mutah.edu.jo or al-madanat@iftc.uni-hannover.de (O.Y.A.-M.); fethi_kooli@yahoo.com (F.K.)

Abstract: Na-kenyaite materials are available in nature and can easily be prepared in the laboratory. These materials exhibit interesting adsorption properties; therefore, they can be invested in the new wastewater treatment technologies. This study investigates the removal of basic blue-41 (BB-41) dye from artificially contaminated water using Na-kenyaite materials in batch mode. Firstly, Na-kenyaites were prepared by the hydrothermal process at a temperature of 150 to 170 °C for a period of 2 to 7 days using different silica sources and ratios of $SiO_2/NaOH/H_2O$. The prepared materials were characterized by different techniques such as XRD, FTIR, ^{29}Si MAS NMR, TGA/DTA, SEM, and nitrogen adsorption isotherms. A pure Na-kenyaite phase was successfully obtained using a fumed silica source and $5SiO_2/Na_2O/122H_2O$ ratio. The removal experiments of basic blue-41 estimated the effectiveness of Na-kenyaites in removing properties, investigating the influence of the solid dosage, initial basic blue-41 concentration, and solution pH or Na-kenyaite solid. Results showed optimal dye removal of around 99% at pH levels above 7. Furthermore, the estimated maximum removal capacity from the Langmuir isotherm was between 124 and 165 mg/g. The results demonstrated efficient removal by Na-kenyaites and its prominence for wastewater treatment. Finally, this study explored the regeneration and reuse of Na-kenyaites through seven cycles and reported a design of a batch adsorber system to reduce the initial concentration of 200 mg/L at different percentages.

Keywords: basic blue-41; hydrous layered silicates; Na-kenyaite; single-batch design; regeneration; removal

Citation: Al-Madanat, O.Y.; Popoola, S.A.; Al Dmour, H.; Al-Faze, R.; Kooli, F. Na-Kenyaite as Efficient Basic Blue-41 Dye Removal: Synthesis and Regeneration Studies. *Water* **2024**, *16*, 2056. https://doi.org/10.3390/w16142056

Academic Editor: Laura Bulgariu

Received: 14 June 2024
Revised: 8 July 2024
Accepted: 17 July 2024
Published: 20 July 2024

1. Introduction

Water resources are crucial to human survival and well-being [1]. Over the past century, water consumption has grown twice as fast as the total population. Due to the dramatic increase in water consumption and issues such as water pollution, water scarcity has become a major challenge facing humanity. Various water and environmental pollutants [2], such as heavy metals [3], polycyclic aromatic hydrocarbons, dyes, pesticides, phenols, etc., are major causes of water crises and waterborne diseases as they can be transmitted to humans through the food chain [4–10]. Hence, a sustainable supply of clean water and conventional wastewater treatment technologies are required to meet the basic domestic and industrial needs.

Thousands of different types of dyes are synthesized and used in various types of industrial processes. The dye molecules are considered a threat to the aquatic environment; therefore, several research groups are still focusing on making a safe environment from the contaminated effluents. Basic blue-41 is a kind of basic dye; once it is dissolved in water, it will acquire a positive charge and make its removal easy by the negatively charged surface of the removal agents. Different methods for remediation of dye-containing wastewater

are reported and reviewed in many reviews [1,11,12], showing that each method has its advantages and drawbacks [12]. Among them, the adsorption process has shown promising potential for the remediation of these dyes from wastewater [1,13]. BB-41 is used in different applications and many researchers are focused on its remedial using different materials, as shown in Table 1.

Table 1. The removal properties of some silicate layered materials for BB-41.

Used Material	Removal Efficiency (mg/g)	Ref.
Na-magadiites	150–220	[14]
Sol-gel silica synthesized from grape bagasse	268	[15]
Saudi Arabia-local clay mineral	74	[16]
Clinoptilolite/Fe_3O_4 nanoparticles	192	[17]
Brick waste materials	60–70	[18]
Silica nanoporous particles	345	[19]
Mn-modified diatomite	62	[20]
Zeolite tuff	93	[21]
Natural Gordes zeolite	149	[22]

Hydrous layer silicates (HLSs) are still gaining a lot of interest in point-of-view academic and industrial research due to their unique physical and chemical characteristics. One member of the group of HLSs is kenyaite, with a general chemical formula of $NaSi_{11}O_{21}(OH)_4 \cdot 3H_2O$. Other formulae were also reported in the literature, and they depend on the preparation conditions [23–26].

The silicate layers are composed of interconnected [SiO_4]-units that contain equal numbers of terminal silanol/siloxy groups on either side of the layer. The cations of low charge density are intercalated between the layers in addition to water molecules [27]. The hydrothermal method is the most widely established method due to its ease of synthesis as well as separation [28]. Depending on the required final product, such as the phase type, purity, and high crystallinity, the conditions of the hydrothermal such as the silica source, the ratio of $SiO_2/NaOH/H_2O$, and the temperature are tuned [14,29,30]. In some cases, the varied combinations of cations in the silicate materials can be utilized to acquire desired properties. Na-kenyaite was also prepared in the presence of ethylene glycol [31–33].

The potential cation exchange properties make Na-kenyaites extremely useful for a wide range of applications. Na-interlayer exchangeable cations cause the adsorptive removal of charged contaminants from wastewater, such as metals [29,34], organic pollutants, and dyes [35]. Other applications of these silicates were also reported. Na-kenyaite was employed as a precursor for the preparation of porous-layered carbon by using PFO (pyrolyzed fuel oil) [36], and for some catalytic purposes [33,37].

The surface properties of Na-Kenyaite could be altered by different means, either by intercalation of some organic molecules between the layer silicates, by insertion of some metals in the silicate layers during the synthesis, or by functionalization of the surfaces [38]. The method of modification depends on the aim of the application. Indeed, for the removal of acidic dyes, the conversion of Na-kenyaite to organophilic material was adopted [35]. According to reported studies, the Na-kenyaite results from the conversion of Na-magadiite to Na-kenyaite by increasing the synthesis temperature from 150 °C to 170 °C [24,31,39]. By adjusting the starting composition of the gel, the Na-Kenyaite is prepared directly without the formation of Na-magadiite as an initial stage [40].

In the case of silicate layered silicates, the removal amount depends on the cation exchange capacity of the used solid and not on the surface areas. Na-kenyaite exhibits a theoretical cation exchange capacity (CEC) value of 130 meq/100 g [41], higher than alumino-silicate layered materials. Thus, it will be worth investigating its removal properties for a selected BB-41 dye.

BB-41 is a common industrial dye that poses a significant threat to aquatic ecosystems due to its persistence and potential toxicity. This study investigates the potential of Na-kenyaite, a layered silicate with a high cation exchange capacity, for the removal of BB-41

dye from wastewater. Na-kenyaite has previously shown promise in removing other pollutants, but its application for the removal of BB-41 is not well-explored and studied. Thus, this study focuses on the synthesis of the pure Na-kenyaite phase from different silica sources at different conditions, including an intermediate conversion of Na-magadiite to Na-kenyaite or direct synthesis without passing through the intermediate conversion at mild conditions. Different physicochemical techniques were utilized to characterize the prepared Na-kenyaites. The removal of BB-41 dye was undertaken using the Na-kenyaite materials, and the maximum removal amount was achieved by optimizing the favorable conditions. The effects of removal parameters were investigated. The regeneration of spent selected kenyaites was examined using the oxone process [42]. A single-batch adsorber design was suggested for selected Na-kenyaite materials, and the Langmuir isotherm parameters were used to estimate the masses required to reduce the 200 mg/L initial concentration of BB-41 dye to 20 mg/L.

2. Materials and Methods

2.1. Materials

Sodium hydroxide and the different silica sources such as Ludox HS-40% (HS), Ludox AS-40% (AS), fumed silica (FS), and colloidal silica (CS) were purchased from the Sigma-Aldrich company (St. Louis, MO, USA). Cobalt nitrate salt, oxone, and BB-41 dye were acquired from Across Organics (Geel, Belgium). All the chemicals used in the synthesis or experimental processes were used as received in their original form.

2.2. Preparation of Na-Kenyaite

A typical mixture was prepared by dissolving 4.80 g of NaOH in 105.00 g of distilled water, then 45.00 g of fumed silica (or other silica source) was added to the sodium hydroxide solution with stirring for over 30 min. The resulting mixture had a molar composition of $Na_2O/5SiO_2/122H_2O$, and it was further stirred for another 1 h at room temperature. Finally, it was transferred into a Teflon liner autoclave at 150 °C for 7 days in a dry static oven. After that, the autoclave was quickly quenched in an ice bath, and the sample was separated using filtration and washed with distilled water until a neutral pH before being air dried at 40 °C overnight [14].

In some cases, the amount of used water was changed from 10.00 g to 40.00 g, and the other variables were kept constant (4.80 g of NaOH and 45.00 g of fumed silica), including the temperature of 150 °C for 2 days. Table 2 provides information on the various compositions used.

Table 2. Na-kenyaite phase obtained at various compositions of reactants and conditions of synthesis.

Run	Silica Source	NaOH (g)	SiO_2 (g)	H_2O (g)	Temp (°C)	Time (h)	Phase	Assignment
1	Fumed Silica	4.80	45.00	105.00	150	7	[1] Ken	KEN-FS-150-7d
2		4.80	45.00	105.00	150	10	Ken + silica	KEN-FS-150-10d
3		4.80	45.00	105.00	170	2	Ken	KEN-FS-170-2d
4		4.80	45.00	20.00	150	2	Ken	KEN-FS-150-20W
5		4.80	45.00	10.00	150	2	[2] Amp silica	KEN-FS-150-10W
6		4.80	45.00	40.00	150	2	Ken + mag	KEN-FS-150-40W
7	Colloidal Silica	4.80	45.00	105.00	170	2	Ken	KEN-CS-170-2d
8		4.80	45.00	105.00	150	7	Ken + silica	KEN-CS-150-7d
9	Ludox-HS 40%	4.80	45.00	105.00	150	7	Traces Ken + silica	KEN-HS-150-7d
10	Ludox-AS 40%	4.80	45.00	105.00	150	10	[3] Mag + Ken + silica	KEN-AS-150-7d

[1] Ken: Kenyaite; [2] Amp: Amorphous; [3] Mag: Magadiite.

2.3. Characterization Techniques

An X-ray diffractometer, Advance8, Bruker (Karlsruhe, Germany) equipped with CuK radiation (λ = 1.5406 Å) was used to acquire the powder XRD patterns (PXRD) through-

out the 2θ range of 2–50 degrees in order to explore the crystallographic and structural information of as-prepared samples. The solid was heated at the rate of 10 °C/min to perform the thermogravimetric and differential thermal analysis (TGA/DTA) using air atmosphere. The analysis was performed with a temperature range spanning from 25 °C to 900 °C, utilizing equipment from TA Instruments (New Castle, DE, USA). All FTIR studies were carried out using a spectrophotometer-6700 Shimadzu (Kyoto, Japan) in the range of 400–4000 cm^{-1} employing the KBr pellet technique. Bruker 400 spectrometer (Karlsruhe, Germany) was employed to collect the solid ^{29}Si magic angle spin (^{29}Si MAS NMR) spectra [14]. The surface morphologies were performed by scanning electron microscopy (SEM), a Jeol model JSM-6700F (Tokyo, Japan). N_2 gas adsorption–desorption isotherms were measured at −196 °C employing the Quantachrome Instrument (Boynton Beach, FL, USA). Treatment of the samples was undertaken by an outgassing process at 150 °C for 3 h prior to the analysis. The specific surface area (SSA) was determined using the Brunauer–Emmett–Teller equation, and the pore volume was estimated at a relative pressure of 0.95 using the adsorption branch.

2.4. Batch Removal of Basic Blue-41

In order to assess the removal effectiveness, 0.10 g of Na-kenyaite was added to 12.00 mL closed tubes containing 10.00 mL of a predetermined concentration of BB-41 solution with different concentrations ranging from 25 to 1000 mg/L. The mixture was shaken overnight at 120 rpm using a water-controlled shaker at 25 °C. Using the UV-1800 spectrophotometer (Shimadzu, Kyoto, Japan) with a wavelength of 610 nm, the remaining quantity of BB-41 dye in the solution was measured. The capacity of BB-41 removal and efficiency were calculated. Different factors included the dosage of Na-kenyaite (0.0050–1.00 g), the initial concentration of dye (25–1000 mg/L), the pH of the cationic dye solution (2–11), and the morphology of the Na-kenyaite materials was investigated to achieve the optimum conditions for high removal efficiency values.

The removal percentage ($R\%$) and removed amount of BB-41 (qe in mg/g) were estimated from Equations (1) and (2), respectively:

$$R\% = \frac{(C_i - C_e) * 100}{C_i} \quad (1)$$

$$qe = (C_i - C_e) * \frac{V}{M} \quad (2)$$

where C_i and C_e correspond to initial and equilibrium concentrations in mg/L. M is the used mass (g) of the solid, and V is the volume (L) of BB-41.

For the estimation of the isotherm parameters (q_{max} (mg/g) and K_L (L/mg)), both Langmuir linearized (Equation (3)) and non-linearized (Equation (4)) plots were used.

$$\frac{C_e}{q_e} = \frac{C_e}{q_{max}} + \frac{1}{q_{max}.K_L} \quad (3)$$

$$qe = \frac{q_{max}.K_L.C_e}{(1 + K_L.C_e)} \quad (4)$$

2.5. Regeneration Tests

The regeneration experiments were carried out using a mixture of cobalt nitrate and oxone solutions, as reported in previous studies [16]. Selected Na-kenyaite samples were treated first with a fresh solution of BB-41 (50 mL with C_i of 200 mg/L) for 8 h at room temperature. The fresh spent materials were separated by centrifugation and treated with a solution composed of oxone and cobalt nitrate (pH 5.1) for 30 min, separated from the solution, and rinsed with deionized water. It was reused in the next cycle. UV spectrophotometer was employed to estimate the concentration at equilibrium (C_e), and

thus, the adsorption efficiency percentage was determined. A similar procedure was carried out for the second and other cycles.

2.6. Theoretical Calculation

The computations were made with a P4 Duo Processor X64 (8G RAM) microcomputer in Windows 8.0 environment. All calculations were made using HyperChem v7 software "http://www.hypercubeusa.com, accessed on 5 January 2024. The geometry of basic blue-41 was optimized at the MM+ level of theory (r.m.s = 0.00941 kcal/mol/Å). Mulliken atomic charges and electrostatic potential were assessed by the semi-empirical parametric method 3 (PM3), being derived from the Hartree–Fock theory.

3. Results and Discussion

3.1. Characterization of Na-Kenyaite Synthesized Materials

During the synthesis trials, Na-magadiite and Na-kenyaite were the two primary phases that were identified. The experiments in this study are focused on Na-kenyaite. The structure was made up of 15.9 Å thick stacked silicate layers, with sodium ions and water molecules occupying the interlayer voids. The 5- and 6-membered rings (R5) and (R6) in the dense layers have a topology similar to the layers found in RUB-6. The Na-kenyaite exhibited no porosity, and its silicon Q^4 to Q^3 ratio was 4:1. Strong reflection was seen in the PXRD pattern at a distance of almost 2.00 nm, besides other broad reflections but with varied half-widths [27].

As indicated in Table 2, pure Na-kenyaite was difficult to synthesize from Ludox HS-40% and Ludox AS-40% with an additional phase of silica at 150 °C and a period of reaction of 7 and 10 days, or at 130 °C for 10 days. However, the pure Na-kenyaite phase was achieved using the starting material colloidal silica at 170 °C for 48 h (2 days). The temperature of synthesis could be decreased to 150 °C starting from fumed silica for a longer period of 7 days. Na-kenyaite was partially converted to the silica phase for a longer period of 10 days.

By optimizing the reaction conditions, in this work and for the first time, the pure Na-kenyaite phase was synthesized at a lower temperature via the hydrothermal treatment at 150 °C with a short period of 2 days by decreasing the water content in the gel from 105.00 g to only 20.00 g. By decreasing the water content to 10.00 g, however, only the amorphous silica phase was obtained. Recently, by adding 40.00 g of water to the gel, a partial conversion of Na-kenyaite to Na-magadiite occurred [14]. Generally, the conversion of Na-magadiite to Na-kenyaite was reported [24]. However, in the present study, Na-kenyaite was partially converted to Na-magadiite by tuning the water content in the gel mixture. Any attempts to raise the temperatures between 180 and 200 °C did not lead to the formation of Na-kenyaite under the present experimental conditions. Recently, Ariyapala et al. [30] reported the synthesis of the Na-kenyaite phase hydrothermally at 190 °C for 1 day by employing amorphous silica sources in the presence of different water-to-NaOH ratios.

The PXRD patterns of the as-prepared materials synthesized at different conditions (Table 2) are depicted in Figure 1. The patterns are consistent with the reported pattern of Na-kenyaite (JCPDS-ICDD No: 20-1157). The intense (001) reflection in the range of 1.96 nm to 2.01 nm, associated with several (00l) reflections, indicates a well-crystalline Na-kenyaite phase (Figure 1a–d). In certain cases, the silica phase was detected as an impurity (Figure 1b) or as the dominant phase (indicated as a star in Figure 1e); the position of this reflection was found in agreement with several previously reported values by other research groups [29,38,43]. It was stated that this position was related to the intercalated cations between the silicate layers of kenyaite [25] and the contents of water between the silicate layers [30,35].

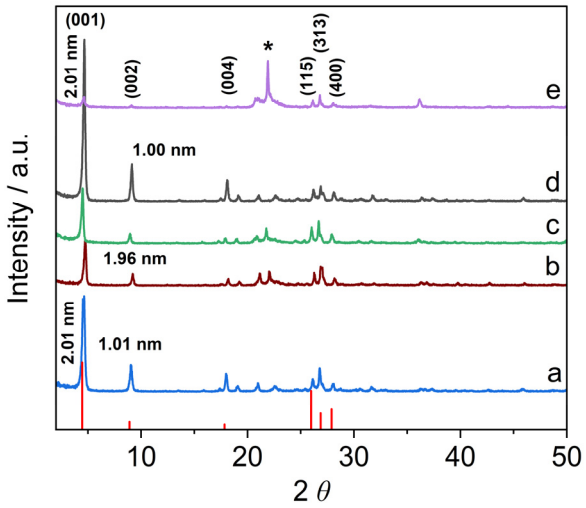

Figure 1. PXRD patterns of as-synthesized materials: (a) KEN-FS-150-7d, (b) KEN-CS-150-7d, (c) KEN-CS-170-2d, (d) KEN-FS-170-2d, and (e) KEN-HS-150-7d. (*) indicate the pattern of silica phase. The reference patterns of the Na-kenyaite (JCPDS-ICDD No: 20-1157) are represented by red bars. (For the identification of samples, please check Table 2.)

As mentioned in Table 2, the water content affected the Na-kenyaite synthesis phase, and the PXRD patterns of the synthesized samples are depicted in Figure 2.

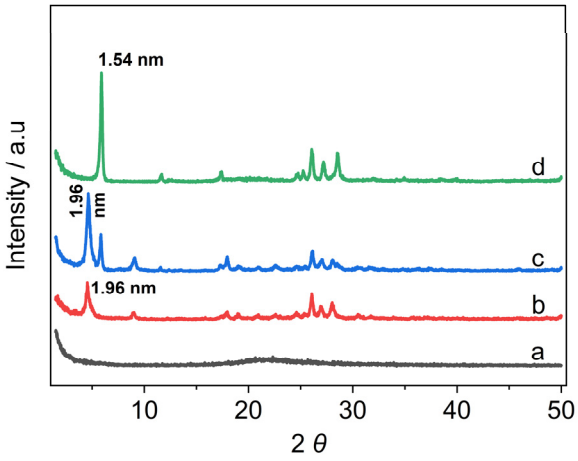

Figure 2. PXRD patterns of materials prepared at different contents of water: (a) 10.00 g, (b) 20.00 g, (c) 40.00 g, and (d) 50.00 g.

Figure 2b exhibited the characteristic reflections for the Na-kenyaite sample prepared using 20.00 g of water at 150 °C for 2 days (JCPDS-ICDD No: 20-1157). An amorphous silica phase was obtained by decreasing the water content to 10.00 g (Figure 2a). However, when increasing the content of water to a total from 30.00 to 40.00 g, an additional Na-magadiite was observed with an intense reflection of 1.56 nm (Figure 2c). The Na-kenyaite was completely transformed to a magadiite phase for higher contents of 50.00 g of water and above in the initial gel (JCPDS-ICDD No:42-1350) (Figure 2d).

Scherrer's equation was used to estimate the crystallite size from the position of 001 reflection and its FWHM. The data indicated that the crystalline size of KEN-FS-150-7d increased from 121 nm to 140 nm as the temperature rose from 150 °C to 170 °C (KEN-FS-170-2d). For longer periods of synthesis at 150 °C, the crystallite size of KEN-FS-150-7d decreased from 121 nm to 105 nm (KEN-FS-150-10d). Interestingly, Na-kenyaite prepared with a lower amount of water (KEN-FS-150-20W) exhibited the smallest crystalline size of

70 nm. The type of silica source did not affect the crystallite phase. Na-kenyaite prepared from fumed or colloidal silica exhibited a similar crystallite size of 140 nm.

Figure 3 displays typical TGA (Figure 3A) and the derivative DTG (Figure 3B) features for Na-kenyaite synthesized from fumed silica at different conditions. Na-kenyaite's TGA characteristic showed three different mass loss stages. The loss of water absorbed on the surface of 4.47% within the 25–100 °C range is related to the DTG temperature peak at 85 °C. Following, the 3.90% mass loss between 100 °C and 150 °C can be attributed to the loss of intercalated water and strongly bonded water molecules to Na^+ cations, which was associated with two DTG peaks at maximum temperatures of 112 °C and 126 °C, respectively. At temperatures beyond 200 °C, a weak third mass steep of 0.77% was attributed to the silicate's dehydroxylation of the silicate layers that occurred at a maximum temperature of 280 °C.

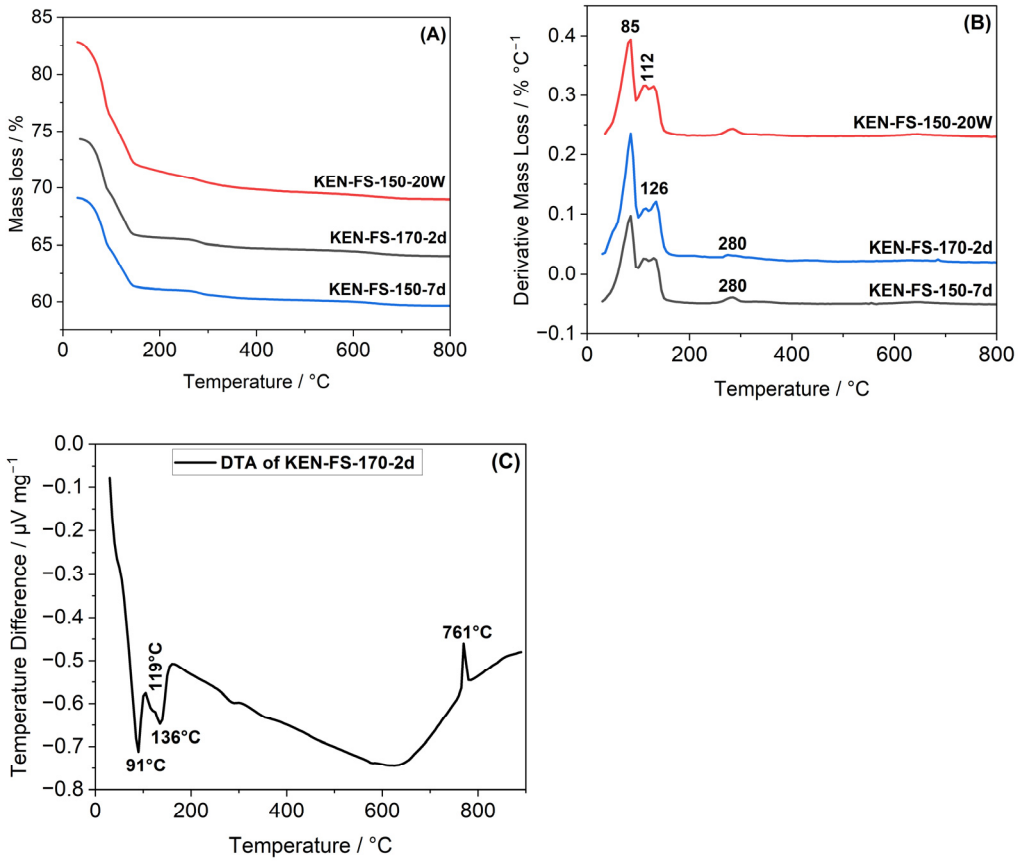

Figure 3. Typical TGA (**A**), the derivative DTG (**B**) features for Na-kenyaite synthesized from fumed silica at different conditions, and the DTA curve of KEN-FS-170-2d (**C**).

The present TGA/DTG characteristics features were comparable to those reported for similar kenyaite materials [25,29,44]. For the other as-prepared Na-kenyaite materials under different conditions, the features are similar, with a slight variation in percentage mass losses. Thus, they clearly exhibit and confirm the kenyaite character of the synthesized products. Indeed, the characteristics of TGA/DTG of the synthesized materials matched those of comparable Kenyaite minerals that were previously described [25,29,44]. Furthermore, we observed that the synthesized Na-kenyaite with the least water content (KEN-FS-150-20W) had shown the lowest total mass loss in the 25–800 °C temperature range.

Figure 3C displays the DTA curve of a Na-kenyaite sample synthesized at 170 °C for 2 days (KEN-FS-170-2d). It demonstrates that endothermic peaks at 91 °C and 136 °C, with a shoulder at 119 °C, accompany the loss of several types of water molecules. The complete dehydroxylation of the synthesized kenyaite phase and the amorphous silica

phase recrystallization resulted in the observation of an exothermic peak at temperatures around 761 °C [29,44].

According to the in situ XRD study [35], the total loss of water molecules between the layers caused the basal spacing of Na-kenyaite to decrease from 1.97 nm to 1.82 nm at 100 °C. Further, to 1.62 nm above 150 °C up to 400 °C, there were slight variations from 1.63 nm to 1.58 with the decrease of the intensity of the main reflection, associated with the low crystallinity degree of the calcined materials. Even at 400 °C, the reflection at 1.62 nm indicated that intercalated molecules of water were not completely removed. Recently, it was reported that the Na-kenyaite phase was not completely destroyed at 800 °C, and a weak reflection of 1.96 nm was still recorded [14]. Similar data were also reported for other members of the HLS family, such as Na-magadiite [41,45].

The FTIR spectra of the Na-kenyaite synthesized using fumed silica at different conditions are shown in Figure 4. The spectrum of KEN-FS-150-7d (Figure 4a) showed a strong and intense band at 1086 cm^{-1}, with two accompanying shoulders at 1245 and 1175 cm^{-1}. These bands could be assigned to the SiO_2 skeleton of layered structures, corresponding to Si-O-Si asymmetric stretching [29,46,47]. In addition, the recorded band at 1245 cm^{-1} was previously reported for 5 rings (R5s) [47]. The sharp bands at 825 cm^{-1} and the weak ones around 690 cm^{-1} were attributed to Si-O-Si symmetric stretching modes. Meanwhile, Si-O-Si bending deformations of the simple and double rings were attributed to the observed different strength bands at 623 and 486 cm^{-1}. The similar bands in Figure 4a–c at 3640, 3530, and 3354 cm^{-1} represent the typical OH stretching assigned to OH of hydration water and Si-OH. The water's bending deformation bands are identified at 1630 and 1670 cm^{-1} and linked to the hydrogen bonding that formed between the hydration water of sodium cations and free water molecules [48].

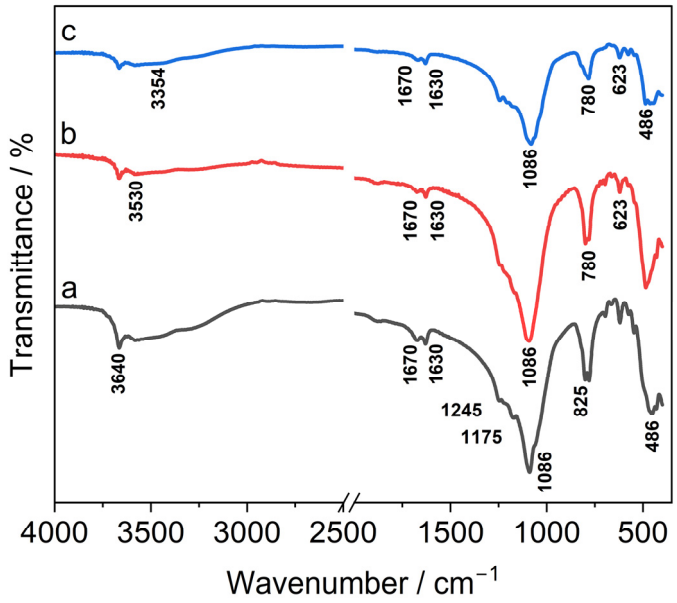

Figure 4. Representative FTIR spectra of (a) KEN-FS-150-7d, (b) KEN-FS-170-2d, and (c) KEN-FS-150-20W.

The FTIR spectra recorded for KEN-FS-170-2d (Figure 4b) and KEN-FS-150-20W (Figure 4c) synthesized Na-kenyaite materials are similar, with some broadness of the characteristic bands due to the crystallinity degree of these materials. Qualitatively, the characteristic bands of the hydroxyls and water molecules decreased in intensity and agreed with the variation in the percentage mass losses related to water molecules.

The ^{29}Si MAS NMR was utilized to support the reported data above. It gives more detailed information about the Si environments in the layered silicate (Figure 5).

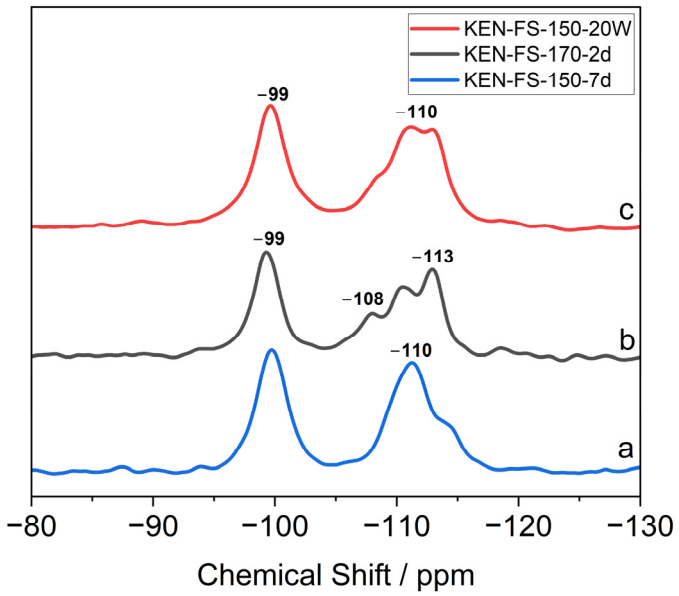

Figure 5. ^{29}Si MAN-NMR spectra of (a) KEN-FS-150-7d, (b) KEN-FS-170-2d, and (c) KEN-FS-150-20W.

Indeed, the spectrum of Na-kenyaite synthesized at 170 °C for 2 days (Figure 5b) exhibited mainly a resonance peak at −99 ppm assigned to Q^3 silicon species and a clear triplet at −108 ppm, −110 ppm, and −113 ppm related to the different types of Q^4 silicon species [49]. Similar features were reported for Na-Kenyaite materials synthesized at different conditions. For example, Na-kenyaite prepared using low content of water at 150 °C for 2 days exhibited the main peak at −99 ppm, with an overlapping of the Q^4 bands in the range of −120 ppm to −100 ppm [24,27]. The overlapping of Q^4 silicon bands was also reported for similar materials such as Na-magadiites [14,37]. The Q^4-to-Q^3 ratio was computed in the range of 1.00 to 2.00. This result was less than the literature-reported value of about 4.00 [14,27]. Several factors that could affect this ratio were reported for the layered silicates, which are mainly related to the crystallinity of these materials. Thus, using this technique indicated that the content of the water used for the synthesis of the Na-kenyaite affected the crystallinity degree and supported our PXRD-collected data.

Based on the SEM analysis in Figure 6, Na-kenyaite synthesized for 7 days at 150 °C (KEN-FS-150-7d) exhibited a hexagonal platy shape with varied-sized crystals, and some lamellar domains were seen locally (Figure 6a). In some cases, the rosette-like morphology was reported for this material prepared at different conditions and using Na_2CO_3 [29,48]. Since the Na-kenyaite was a result of the transformation of Na-magadiite, the morphology of Na-kenyaite was reported to be similar to Na-magadiite [24]. The used amount of water was reported to affect the morphology of this kind of layered silicate. Indeed, the colly flower morphology was converted to a platy layered structure in the case of Na-magadiite [14]. However, in the case of Na-kenyaite prepared using a lower amount of water (20.00 g, KEN-FS-150 20W, the material exhibited stacked plates with different shapes (Figure 6b). In some cases, a twisted morphology of these plates was achieved. For Na-kenyaite prepared at 170 °C for 2 days (KEN-FS-170-2d), plates with hexagonal shapes of different sizes are observed, staked with some voids between them (Figure 6c).

We observed that the corresponding Na-kenyaite that formed by using colloidal silica exhibited a similar morphology to the materials prepared using a fumed silica source. However, different morphologies were reported for the same types of materials [50–52]. These observations lead us to conclude that the synthesis conditions impacted these morphologies, and one has to take care of the synthesis conditions to compare the obtained data.

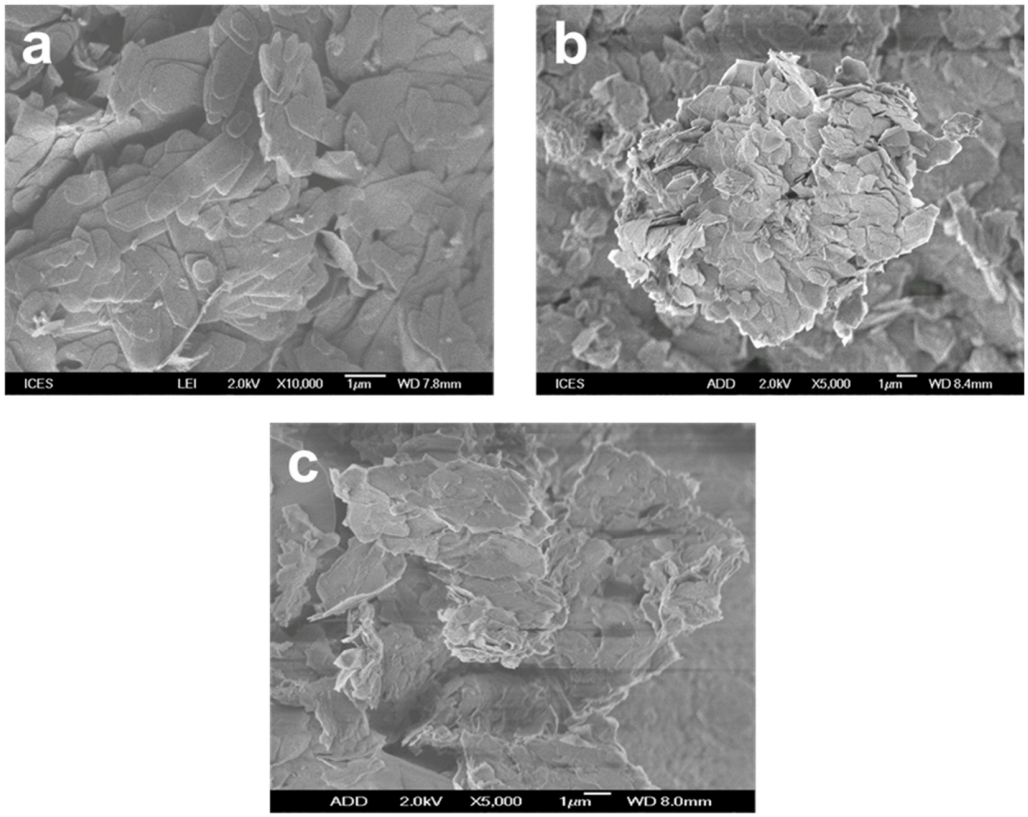

Figure 6. SEM micrographs of (**a**) KEN-FS-150-7d, (**b**) KEN-FS-150 20W, and (**c**) KEN-FS-170-2d.

The measured surface area (SSA) values of the different synthesized Na-kenyaites ranged from 25.00 to 30.00 m^2/g. These values were higher than the reported ones in the literature for similar materials (11.00 m^2/g) [44]. Our results showed that the SSA was not greatly impacted by the synthesis conditions. These results may suggest that most of the nitrogen molecules were adsorbed on the exterior surface of the layered silicates and that not all nitrogen molecules have access to all of the adsorption sites for nitrogen probe molecules. Analogous information was documented about hydrous layered silicates, including Na-magadiite [27,53,54]. The estimated total pore volumes of the various Na-kenyaites were found to be in the range of 0.20 to 0.25 cc/g. The average pore widths were linked to the spaces between the Na-kenyaites' particles because these materials showed no signs of porousness.

3.2. Removal Properties of Basic Blue-41

3.2.1. Effect of Initial Concentrations

A range of BB-41 concentrations, between 25 and 1000 mg/L, were utilized to assess how the removal properties of particular Na-kenyaite were affected by the initial concentrations. In this case, the other variables remained unchanged, such as the pH used mass of 0.01 g, volume of BB-41 solution (10.00 mL), and temperature of 25 °C. The results that were calculated based on Equations (1) and (2) show that as the initial concentrations increased, so did BB-41 uptake by KEN-FS-150-7d (Figure 7).

The solution with an initial 25 mg/L of dye had the least quantity eliminated, whereas the solution with a 1000 mg/L concentration exhibited the highest quantity removal. The percentage removal fell from 100% to 29%, while the BB-41 Ci levels increased simultaneously. As additional removal sites were accessible, the quantity of removal increased. Through mass driving forces, the enhanced interactions between BB-41 molecules and Na-kenyaite probably contributed to the improvement in adsorption capacity [55,56]. Similar observations have been reported for many silicates with various cationic dyes. A 42%

decrease in the removal percentage was reported for Na-magadiite, and a 32% decrease was reported for Saudi Local Clay Mineral using the same BB-41 dye [14,16].

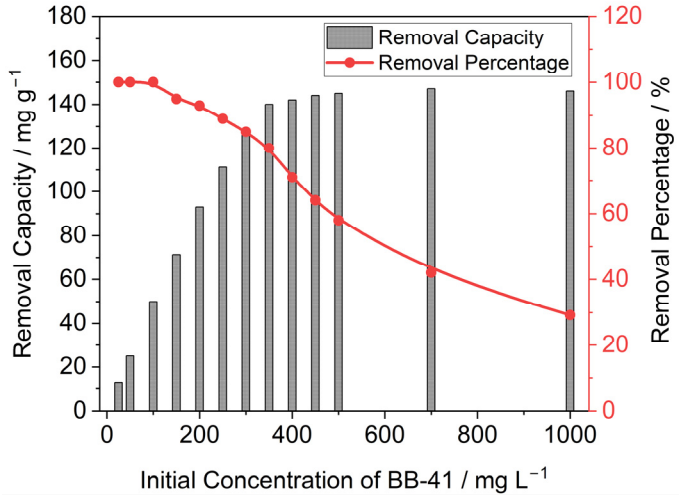

Figure 7. Variation in the removal capacity qe (bar) and removal percentage (red line) with the initial concentration (Ci) of BB-41. Reaction conditions: 0.01 g of KEN-FS-150-7d, 10.00 mL of BB-41 solution, and an overnight contact period at 25 °C.

The number of binding sites remained unchanged, along with the fixed amount of Na-kenyaite. The reduction in removal percentage resulted in the lack of binding sites necessary for the BB-41 molecules at higher initial concentrations. However, more binding sites were available for fewer adsorbate species at lower initial concentrations; therefore, all the dye molecules were removed.

3.2.2. Effect of pH

Effect of BB-41 Solution

It is well known that the pH significantly impacts the surface charge of layered silicates such as Na-magadiite, and the BB-41 ionic species present during dye removal form an aqueous solution [14,29]. Therefore, by using 0.100 g of Na-kenyaite with a C_i of 200 mg/L and an overnight contact period at 25 °C, the influence of pH on the level of dye removal was examined in the range of 2 to 11. Figure 8A demonstrates how the BB-41 solution's original pH affected the BB-41 removed. When the pH was raised from 2 to 10, it was found that the elimination of BB-41 dye increased from 35 to 95%.

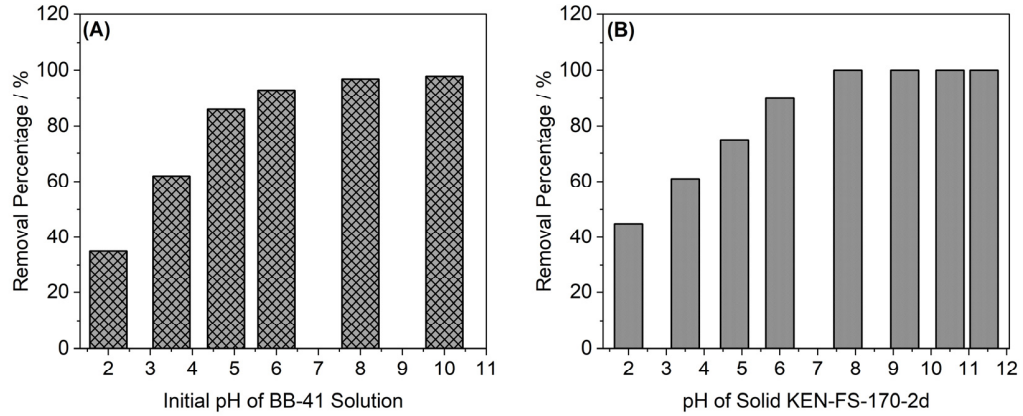

Figure 8. Variation in BB-41 removal percentage with (**A**) initial pH of BB-41, and (**B**) effect of the solid KEN-FS-170-2d pH. Reaction conditions: 0.01 g of KEN-FS-150-7d, 10.00 mL of 200 mg/L BB-41 solution, and an overnight contact period at 25 °C.

At pH 11, the harmful precipitation of dye occurred, and no run was performed at pH higher or equal to 11 [14,29,57]. The initial pH controls the protonation of the BB-41 dye's functional sites and modifies the surface charge of Na-kenyaite by influencing the surface sites by protonation and dissociation [58]. Thus, the reported outcomes can be explained based on the pH_{PZC} value of Na-kenyaite. The pH_{PZC} of Na-kenyaite was measured by the drift method, and it was close to 8. This value was similar to that reported for another layered silicate, Na-magadiite [14]. These two materials were prepared at similar chemical compositions but under different conditions. At pH < pH_{PZC}, the surface of Na-kenyaite acquired a positive charge, and the formation of positively charged species (H_3O^+ or H^+) in the aqueous solution generates repulsive forces with cationic BB-41 dye molecules. This results in a decrease in the removal percentage of the dye in the acidic pH range between 2 and 4. However, the surface of Na-kenyaite is coated with negatively charged functional sites above pH_{PZC}, which enhances electrostatic interaction with the cationic BB-41 dye molecules as the pH of the solution rises, thus leading to a steady increase in dye removal. Alanazi et al. [14] reported a similar removal trend in the case of Na-magadiite. Taking into consideration the optimal removal of the BB-41 dye (85.47%) and avoiding its harmful precipitation, further experiments were performed at natural pH (without altering the pH of the BB-41 solution).

Influence of Na-Kenyaite Solid pH

As previously mentioned, the dye solution's pH was often adjusted at different pH values between 2 and 11 by adding diluted HCl and NaOH solutions before adding the solid material. However, in this investigation, an alternate approach was put out, which involved treating the Na-kenyaite solid in either basic or acidic solutions before adding it to the BB-41 solution of 200 mg/L. The basal spacing of 2.01 nm shrinks to 1.60 nm due to the exchange of Na+ cations by protons using concentrated HCl solution (3.00 M and above), as mentioned in previous studies. The Na-kenyaite was stable in the basic solution, which is not the case for the HCl acidic solution. Here, a few measures and precautions need to be taken into account.

Figure 8B shows that the basic treatment of Na-kenyaite removed approximately 95% of BB-41, while the acid-treated Na-kenyaite removed approximately 45% of BB-41 using a mild HCl solution (0.50 M). The percentage of BB-41 removal reached 100% for Na-kenyaite treated with concentrated NaOH solution (2 M or above). This surprising enhancement was due to the high pH value of the resulting solid, thus affecting the BB-41 pH solution. Indeed, the high basic property of Na-kenyaite/water medium can lead to such phenomena. In this case, the Na-kenyaite/water suspension produces a pH value of more than 10. Previously, a very close value was reported for Na-magadiite [14]. On the other hand, when the acidic pH value of Na-kenyaite was added to the BB-41 solutions, the suspension's final pH value was found to be between 7.50 and 8.00, thus affecting the percentage of BB-41 removal. A similar behavior was reported in the presence of methylene blue (basic dye) and Na-magadiite [59]. It was found that the % elimination increased as the pH increased. Hence, an 8.50 to 10.00 pH interval was found to be the best for MB adsorption on the surface of Na-magadiite [59,60]. In this case, the experimental methods and conditions must be optimized and unified very well for comparison purposes.

3.2.3. Effect of Na-Kenyaite Dosage

The effect of Na-kenyaite doses on BB-41 removal efficacy was explored by escalating the amount from 0.010 g to 1.00 g under fixed reaction conditions—10 mL of 200 mg/L dye concentration at 25 °C and an overnight contact period—while the pH of BB-41 solution was not adjusted and was used as is. The value was found to be between 5.4 and 5.7. It was noticed that the dye removal enhanced to 93% when the Na-kenyaite was increased from 0.010 g/10 mL to 0.100 g/10 mL (Figure 9). At higher doses, the increased surface area of Na-kenyaite results in more active sites; hence, more BB-41 removal was accomplished. It was established that the 0.40 g of solid attained optimal adsorption of 98%, after which

the adsorbent amount did not significantly affect the adsorption. Further dose increments of Na-kenyaite (from 0.40 g to 1.00 g) showed only a minor enhancement in dye removal performance due to the agglomeration of the surface-active site with the increase in the solid dose [14,19]. Therefore, the optimal clearance of BB-41 was achieved at a 0.10 g/10 mL dose of adsorbent, which was then utilized in further experiments.

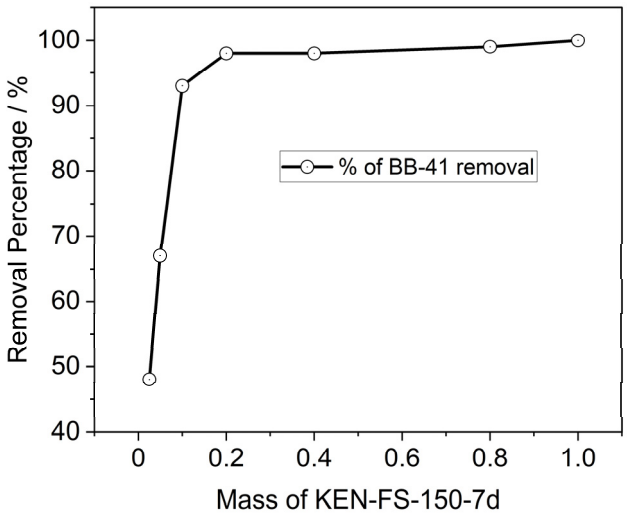

Figure 9. Variation in BB-41 removal (%) with a different amount (g) of KEN-FS-150-7d. Reaction conditions: 10.00 mL of 200 mg/L BB-41 solution, neutral pH, and an overnight contact period at 25 °C.

3.2.4. Effect of Na-Kenyaite Morphology

Na-kenyaites with different morphologies were investigated for the BB- 41 removal. It was reported that the morphology of the layered silicates has affected the removal amounts, as in the case of magadiite materials [14]. In the present case, and at the same experimental conditions (used solid of 0.1 g, at a constant temperature of 25 °C and contact time of 18 h, natural pH). Na-kenyaite with platelet morphology (KEN-FS-150-7d) exhibited the lowest removal amount of 123 mg/g. However, the highest value of 151 mg/g was achieved for Na-kenyaite prepared at 170 °C for two days (KEN-FS-170-2d). The removal trials showed that an intermediate value of 135 mg/g was achieved for Na-kenyaite prepared with low contents of water (KEN-FS-150-20W). Meanwhile, for Na-kenyaite prepared from colloidal silica at 170 °C for a period of 2 days (KEN-CS-170-2d), a value of 165 mg/g was achieved.

3.2.5. Langmuir Adsorption Model

Adsorption isotherms are applied to describe the equilibrium adsorption behavior of adsorbate molecules in liquid media on the surface of the adsorbent. Therefore, adsorption data acquired from the effect of BB-41 concentrations have been utilized to explain the equilibrium dye molecules' adsorption on the Na-kenyaite materials. The commonly used isotherm model is Langmuir. In the Langmuir isotherm, a fixed number of localized binding sites on the adsorbent's surface could be covered by a homogenous monolayer, and all sites are deemed equivalent or identical [14,60]. The most common method for determining the model parameters is linear regression. Furthermore, several researchers also applied the non-linear regression method to estimate the parameters of the adsorption isotherm. This approach is occasionally utilized to prevent errors affecting the value of R^2 [60]. In the present study, both Langmuir linearized and non-linearized plots were used to determine the isotherm parameters, as reported in Table 3.

Table 3. Linear and non-linear Langmuir model parameters for the removal of BB-41 for different materials, calculated based on Equations (3) and (4).

Samples	q_{max} (mg/g)	K_L (L/g)	R^2
KEN-FS-150-7d	147.20 (151.10)	0.2433 (0.1166)	0.9997
KEN-FS-170-2d	136.60 (138.60)	0.1137 (0.0955)	0.9997
KEN-FS-150-20W	118.70 (123.70)	0.1046 (0.0621)	0.9993
KEN-CS-150-7d	124.20 (128.20)	0.1095 (0.1023)	0.9995
KEN-CS-170-2d	165.30 (171.30)	0.2764 (0.1542)	0.9997

The Langmuir model more closely fitted the BB-41 dye adsorption data for all applied Na-kenyaites due to its better correlation value (R^2). The calculations indicate that the investigated Na-kenyaites exhibited a maximum BB-41 removal (q_{max}) of 165.30 mg/g. Additionally, it was noticed that the q_{max} of Na-kenyaites was lower than those of the Na-magadiites previously reported [60]. This difference is correlated to the morphology and CEC values of the Na-kenyaites.

The powder XRD diffraction (Figure 10) of Na-kenyaite after the elimination of BB-41 dyes indicated that the structure of Na-kenyaite was stable and there was no change in the basal distance at the low removal amount of BB-41 (Figure 10b). This data could suggest that the BB-41 dyes were adsorbed on the external surface of the silicate layers.

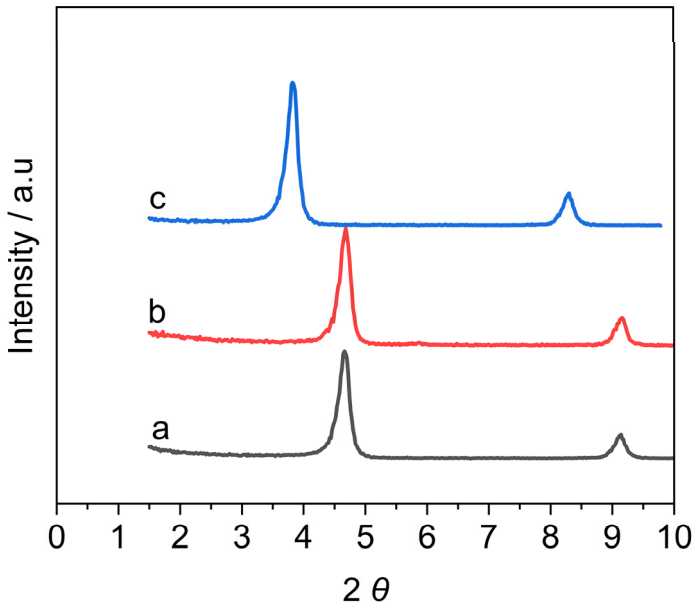

Figure 10. PXRD patterns of (a) pure synthesis KEN-FS-170-2d material, (b) KEN-FS-170-2d with low qe of BB-41, and (c) KEN-FS-170-2d with high qe of BB-41.

At higher uptake values of BB-41 (Figure 10c), the dye molecules were intercalated in the interlayer spacing parallel to silicate layers, and a shift of basal spacing was observed at 2.260 nm. A three-dimensional calculation indicates that the BB-41 dye has a planar structure with the following dimensions: 1.716 nm (length), 0.665 nm (width), and 0.665 nm (thickness). Similar data were reported for the removal of BB-41 molecules by montmorillonite clay mineral [61].

3.2.6. Theoretical Calculation

The Mulliken atomic charges of BB-41 indicated that the majority of the negative charges were concentrated on oxygen and a small number of nitrogen atoms, while on sulfur and more nitrogen atoms, the positive charges were located [57]. Stated otherwise, the half of the molecule containing the heteroatoms of nitrogen and sulfur is more positively

charged. It should be mentioned that the second half of the BB-41 dye molecule has a very strong noticeable positive charge (0.20 e-) on the hydrogen atom of the hydroxyl group (OH).

When BB-41 cations are removed, they are attracted to a negatively charged surface, such as silicate layers, and they will align toward the sides of the surface with the maximum positive charge density. This is known as the electrostatic attraction between the cycle containing the suffer (S) atom or via the hydrogen of the alkyl amine group (-NCH_3) located in the first half of the molecule. Lastly, orientation with the hydrogen of the hydroxyl group on the molecule's second side was not ruled out [57]. In the case of Na-kenyaite, the BB-41 molecules would preferentially align themselves with the sides of the surface that have the highest levels of positive charge density in the event of electrostatic interaction with a negatively charged site on the surface. The orientation via the hydrogen of –NCH_3 (alkyl amine group) was situated in the first half of the molecule or to the orientation, with the cycle having the suffer (S) atom [57,58]. Finally, orientation with the hydrogen of -OH (hydroxyl group) on the second side of the molecule was not excluded. In all cases, the orientation positions of BB-41 are parallel concerning the negatively charged surface of other materials, as confirmed by PXRD data.

3.2.7. Regeneration Studies

In order to make the removal process economically viable and practically applicable, a regeneration study was undertaken. Therefore, experiments on Na-kenyaite materials regeneration were performed at 25 °C for seven cycles using 200 mg/L concentration of BB-41. The following two samples of Na-kenyaites were selected: KEN-FS-170-2d and KEN-FS-150-7d. Figure 11 depicts the regeneration of Na-kenyaite materials for BB-41 dye.

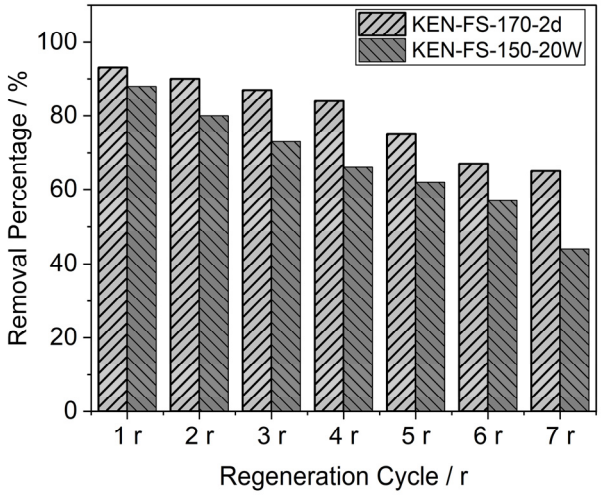

Figure 11. Regeneration tests of KEN-FS-170-2d and KEN-FS-150-20W. Reaction conditions: 100 mg of the solid material, 10.00 mL of 200 mg/L BB-41 solution, pH is 5.1, and an overnight contact period at 25 °C.

The data indicate that KEN-FS-170-2d was used in four regeneration cycles; its removal percentage efficacy decreased from 93% to 84% and then progressively to 73% as the number of regeneration cycles increased. Seven cycles later, the efficacy had dropped to 65%. For KEN-FS-150-20W, the other Na-kenyaite material, the regeneration results showed that this synthesized material lost about 17% of its removal efficacy after the first three cycles, while after the fourth run, its percentage removal reduced gradually, varying from 73 to 66%. However, after the seventh run, 50% of the initial efficacy was still preserved (Figure 11).

The dissimilarity between the two samples could be attributed to the high removal capacity of the KEN-FS-170-2d material, which makes it challenging to break all of the removed BB-41 cations. The morphology of the materials could be opposed to reaching

the removed BB-41 cations, which may be another factor. Similar results were obtained when the same procedure was applied to the regeneration of Na-magadiite and porous clay heterostructure with a large surface area and mesoporous character [57]. In this instance, the catalyst's ability to penetrate the pores and make contact with the BB-41 permitted their decomposition while preserving the effectiveness of the removal process.

Since the Na-kenyaite's synthesis is easy, safe, and affordable, along with its remarkable regeneration, this indicates that it has a good potential to remove BB-41 from an aqueous solution.

It is worth mentioning that before and after regeneration, there was no discernible variation in the PXRD patterns of the regenerated materials. These results demonstrate the stability of the layered silicate under our experimental setup.

3.2.8. Design Single-Stage Batch

Because batch adsorption uses less material and consumes less time, it is preferred in laboratory-scale investigations. However, batch adsorption works well for research on a small scale but is not appropriate for large-scale use. Furthermore, the size and performance of the large batch adsorbers are predicted using laboratory-scale equilibrium studies [62].

Reducing the initial concentration (C_i (mg/L)) of BB-41 solution in volume V (L) to C_1 (mg/L) is the design goal. The removed amount shifts from q_i to q_1 (mg/g), for an M (g) amount of adsorbent. When $t = 0$, $q_i = 0$ (initial removal amount), and time goes on, the mass balance equation reports the amount of BB-41 taken in by the solid, and the amount taken out of the liquid is described in Equation (5) [63]:

$$V(C_i - C_1) = M(q_i - q_1) = Mq_1 \tag{5}$$

The Langmuir isotherm equation can be used for q_1 in the equation batch absorber design because the equilibrium data for BB-41 onto Na-kenyaites fitted well in the model.

The resulting Equation (6) is presented as follows [57]:

$$\frac{M}{V} = \frac{C_i - C_1}{q_1} = \frac{C_i - C_1}{\frac{q_m K_L C_1}{1 + K_L C_1}} \tag{6}$$

The estimated adsorption isotherm parameters reported in Table 3 are necessary to calculate the required solid mass in the single-stage batch design, based on Equation (6).

A sequence of plots showing the expected values of M (g) vs V (L) at the initial concentration of 200 mg/L for 50%, 60%, 70%, 80%, and 90% BB-41 elimination is shown in Figure 12A. For instance, the masses of KEN-FS-170-2d needed to remove 60 and 80% of BB-41 species from 10 L of an aqueous solution were 8.50 g and 17.00 g, respectively.

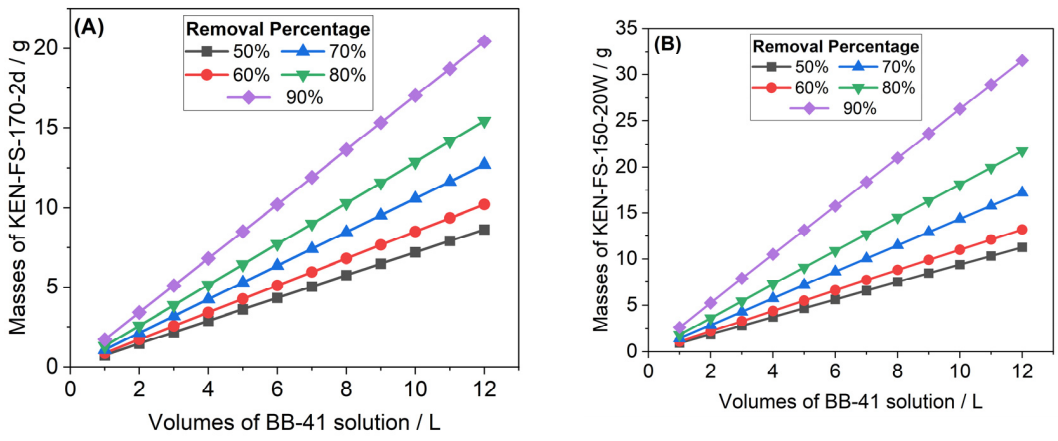

Figure 12. Required masses of KEN-FS-170-2d (**A**) and KEN-150-20W (**B**) to treat different volumes of BB-41 solutions with an initial concentration of 200 mg/L, at different removal percentages.

When the desired reduction in BB-41 concentrations increased, the predicted masses of used Na-kenyaite (KEN-FS-170-2d) increased from 7.20 g to 17.10 g for a fixed volume of 10 L. The predicted masses also increased with the treated volumes of BB-41 at a fixed initial concentration of 200 mg/L (Figure 12B).

In the other case, when Na-kenyaite was prepared with a lower amount of water (KEN-FS-150-20W), the required masses were higher, and the following 9.30 g, 11.10 g, 14.30 g, 18.10 g, and 26.20 g masses were estimated to remove 50%, 60%, 70%, 80%, and 90% of BB-41, respectively, at a 10 L volume of effluent. The difference originated from the variation in the removal capacity of the starting Na-kenyaite. Similar trends were reported for similar hydrous layered silicates such as Na-magadiites or other modified aluminosilicates using BB-41 and eosin-Y dyes [14,57,64]. Both large-scale batch applications and the design of pilot-batch systems become crucial to this evaluation.

4. Conclusions

In the present work, Na-kenyaite materials were prepared and exploited for the removal of the cationic dye basic blue-41. Fumed silica as a source of silica led to reproducible data and the required temperatures were at 150 °C for 7 days or at 170 °C for 2 days. The content of water in the starting reaction mixture was found to play a crucial role; using a water mass of 20.00 g, pure Na-kenyaite was obtained at 150 °C for a short period of 2 days. By adding more water (30.00 g), the transformation of Na-kenyaite to Na-magadiite occurred, and only Na-magadiite was obtained using 40 g of water and above. The removal of BB-41 was evaluated considering the following factors: initial dye concentration, initial pH of BB-41 solution or Na-kenyaite solid, morphology of Na-kenyaite materials, and Na-kenyaite load. The removal percentage rose as the mass of Na-kenyaite increased to the optimal 0.10 g. The percentage removal attained a maximum of 98% at pH 9 for the BB-41 solution, or when the Na-kenyaite was treated with a basic solution before the removal process. The increase in the initial dye concentration resulted in an increase in the removal amounts. The maximum removed amounts of BB-41 were in the range of 118 mg/g to 165 mg/g. The Na-kenyaites could be regenerated up to three to five times before losing about 30% of its efficiency. The batch design results indicate that the predicted masses of used Na-kenyaite depended on the target removal percentage values. Na-kenyaites could be considered a sustainable, efficient, and reusable adsorbent with significant regeneration, which makes it beneficial for the industry and the environment, and could significantly contribute to more sustainable and cost-effective wastewater treatment processes, leading to cleaner water sources.

Author Contributions: Conceptualization, O.Y.A.-M. and F.K.; methodology, O.Y.A.-M., S.A.P., H.A.D., R.A.-F. and F.K.; software, O.Y.A.-M., H.A.D. and F.K.; validation, S.A.P., H.A.D. and F.K.; formal analysis, O.Y.A.-M., S.A.P. and R.A.-F.; investigation, H.A.D., R.A.-F. and F.K.; resources, H.A.D., R.A.-F. and F.K.; data curation, O.Y.A.-M., S.A.P., H.A.D., R.A.-F. and F.K.; writing—original draft preparation, O.Y.A.-M., S.A.P., H.A.D., R.A.-F. and F.K.; writing—review and editing, O.Y.A.-M. and F.K.; visualization, S.A.P., R.A.-F. and F.K.; supervision, O.Y.A.-M., S.A.P. and F.K.; project administration, O.Y.A.-M. and F.K.; funding acquisition, O.Y.A.-M. and F.K. All authors have read and agreed to the published version of the manuscript.

Funding: This research received no external funding.

Data Availability Statement: Data are contained within this article.

Acknowledgments: The author Osama Al-Madanat would like to express his gratitude to the Deanship of Scientific Research at Mutah University, Jordan, for its financial support through research grant 887/2024. This support enabled the purchase of chemicals, consumables, and the execution of various analyses. It is important to note that the funders had no involvement in the study design, data collection and analysis, decision to publish, or the preparation of the manuscript.

Conflicts of Interest: The authors declare no conflicts of interest.

References

1. Al-Madanat, O.; AlSalka, Y.; Ramadan, W.; Bahnemann, D.W. Tio_2 Photocatalysis for the Transformation of Aromatic Water Pollutants into Fuels. *Catalysts* **2021**, *11*, 317. [CrossRef]
2. Ombaka, L.M.; McGettrick, J.D.; Oseghe, E.O.; Al-Madanat, O.; Rieck genannt Best, F.; Msagati, T.A.M.; Davies, M.L.; Bredow, T.; Bahnemann, D.W. Photocatalytic H_2 Production and Degradation of Aqueous 2-Chlorophenol over B/N-Graphene-Coated Cu^0/Tio_2: A Dft, Experimental and Mechanistic Investigation. *J. Environ. Manag.* **2022**, *311*, 114822. [CrossRef] [PubMed]
3. Altarawneh, R.M.; Al-Jaafreh, A.M.; Qaralleh, H.; Al-Qaralleh, O.S. Chemical Profiling of Punica Granatum Peels from Jordan Using Lc–Ms/Ms and Study on Their Biological Activities. *Int. J. Food Sci. Tech.* **2022**, *57*, 5256–5267. [CrossRef]
4. Al-Nasir, F.; Hijazin, T.J.; Al-Alawi, M.M.; Jiries, A.; Al-Madanat, O.Y.; Mayyas, A.; Al-Dalain, S.A.; Al-Dmour, R.; Alahmad, A.; Batarseh, M.I. Accumulation, Source Identification, and Cancer Risk Assessment of Polycyclic Aromatic Hydrocarbons (Pahs) in Different Jordanian Vegetables. *Toxics* **2022**, *10*, 643. [CrossRef] [PubMed]
5. Jiries, A.; Al-Nasir, F.; Hijazin, T.J.; Al-Alawi, M.; El Fels, L.; Mayyas, A.; Al-Dmour, R.; Al-Madanat, O.Y. Polycyclic Aromatic Hydrocarbons in Citrus Fruit Irrigated with Fresh Water under Arid Conditions: Concentrations, Sources, and Risk Assessment. *Arab. J. Chem.* **2022**, *15*, 104027. [CrossRef]
6. Al-Nasir, F.M.; Jiries, A.G.; Al-Rabadi, G.J.; Alu'datt, M.H.; Tranchant, C.C.; Al-Dalain, S.A.; Alrabadi, N.; Madanat, O.Y.; Al-Dmour, R.S. Determination of Pesticide Residues in Selected Citrus Fruits and Vegetables Cultivated in the Jordan Valley. *LWT* **2020**, *123*, 109005. [CrossRef]
7. Lewerenz, L.; Hijazin, T.; Abouzeid, S.; Hänsch, R.; Selmar, D. Pilot Study on the Uptake and Modification of Harmaline in Acceptor Plants: An Innovative Approach to Visualize the Interspecific Transfer of Natural Products. *Phytochemistry* **2020**, *174*, 112362. [CrossRef] [PubMed]
8. Hijazin, T.; Radwan, A.; Lewerenz, L.; Abouzeid, S.; Selmar, D. The Uptake of Alkaloids by Plants from the Soil Is Determined by Rhizosphere Ph. *Rhizosphere* **2020**, *15*, 100234. [CrossRef]
9. Hijazin, T.; Radwan, A.; Abouzeid, S.; Dräger, G.; Selmar, D. Uptake and Modification of Umbelliferone by Various Seedlings. *Phytochemistry* **2019**, *157*, 194–199. [CrossRef]
10. Altarawneh, R.M. Facile Fabrication of New Sensing Platforms Decorated with Quinalizarin and Ptni Alloy Nanoparticles for Highly Sensitive Aluminum Determination. *Microchem. J.* **2022**, *182*, 107944. [CrossRef]
11. Lin, J.; Ye, W.; Xie, M.; Seo, D.H.; Luo, J.; Wan, Y.; Van der Bruggen, B. Environmental Impacts and Remediation of Dye-Containing Wastewater. *Nat. Rev. Earth Environ.* **2023**, *4*, 785–803. [CrossRef]
12. Hung, Y.-T.; Adesanmi, B.; Paul, H.; Huhnke, C. Comparison of Dye Wastewater Treatment Methods: A Review. *GSC Adv. Res. Rev.* **2022**, *10*, 126–137. [CrossRef]
13. Holkar, C.R.; Jadhav, A.J.; Pinjari, D.V.; Mahamuni, N.M.; Pandit, A.B. A Critical Review on Textile Wastewater Treatments: Possible Approaches. *J. Environ. Manag.* **2016**, *182*, 351–366. [CrossRef]
14. Alanazi, A.M.; Al Dmour, H.; Popoola, S.A.; Oudghiri Hassani, H.; Rakass, S.; Al-Faze, R.; Kooli, F. Parameters Synthesis of Na-Magadiite Materials for Water Treatment and Removal of Basic Blue-41: Properties and Single-Batch Design Adsorber. *Inorganics* **2023**, *11*, 423. [CrossRef]
15. Benvenuti, J.; Fisch, A.; dos Santos, J.H.Z.; Gutterres, M. Silica-Based Adsorbent Material with Grape Bagasse Encapsulated by the Sol-Gel Method for the Adsorption of Basic Blue 41 Dye. *Environ. Chem. Eng.* **2019**, *7*, 103342. [CrossRef]
16. Kooli, F.; Liu, Y.; Al-Faze, R.; Al Suhaimi, A. Effect of Acid Activation of Saudi Local Clay Mineral on Removal Properties of Basic Blue 41 from an Aqueous Solution. *Appl. Clay Sci.* **2015**, *116–117*, 23–30. [CrossRef]
17. Afshin, S.; Rashtbari, Y.; Vosoughi Niri, M.; Rehman, R.; Ramavandi, B.; Behzad, A.; Mitu, L. Removal of Basic Blue-41 Dye from Water by Stabilized Magnetic Iron Nanoparticles on Clinoptilolite Zeolite. *Rev. Chim.* **2020**, *71*, 218–229. [CrossRef]
18. Kooli, F.; Yan, L.; Al-Faze, R.; Al-Sehimi, A. Removal Enhancement of Basic Blue 41 by Brick Waste from an Aqueous Solution. *Arab. J. Chem.* **2015**, *8*, 333–342. [CrossRef]
19. Zarezadeh-Mehrizi, M.; Badiei, A. Highly Efficient Removal of Basic Blue 41 with Nanoporous Silica. *Water Resour. Ind.* **2014**, *5*, 49–57. [CrossRef]
20. Kul, A.R.; Aldemir, A.; Koyuncu, H. An Investigation of Natural and Modified Diatomite Performance for Adsorption of Basic Blue 41: Isotherm, Kinetic, and Thermodynamic Studies. *Desalin. Water Treat.* **2021**, *229*, 384–394. [CrossRef]
21. Humelnicu, I.; Băiceanu, A.; Ignat, M.-E.; Dulman, V. The Removal of Basic Blue 41 Textile Dye from Aqueous Solution by Adsorption onto Natural Zeolitic Tuff: Kinetics and Thermodynamics. *Process Saf. Environ. Prot.* **2017**, *105*, 274–287. [CrossRef]
22. Mersin, G.; Açıkel, Ü.; Levent, M. Efficient Adsorption of Basic Blue 41 from Textile Wastewaters by Natural and Magnetically Modified Manisa-Gördes Clinoptilolite. *Chem. Eng. Process.* **2021**, *169*, 108632. [CrossRef]
23. Kosuge, K.; Yamazaki, A.; Tsunashima, A.; Otsuka, R. Hydrothermal Synthesis of Magadiite and Kenyaite. *J. Ceram. Soc. Jpn.* **1992**, *100*, 326–331. [CrossRef]
24. Kooli, F.; Mianhui, L.I.; Plevert, J. Comparative Studies on the Synthesis of Na-Magadiite, Na-Kenyaite and Rub-18 Phases. *Clay Sci.* **2006**, *12*, 25–30. [CrossRef]
25. Beneke, K.; Lagaly, G. Kenyaite; Synthesis and Properties. *Am. Mineral.* **1983**, *68*, 818–826.
26. Wang, Z.; Pinnavaia, T.J. Intercalation of Poly(Propyleneoxide) Amines (Jeffamines) in Synthetic Layered Silicas Derived from Ilerite, Magadiite, and Kenyaite. *J. Mater. Chem.* **2003**, *13*, 2127–2131. [CrossRef]

27. Marler, B.; Grosskreuz, I.; Gies, H. The Crystal Structure of Synthetic Kenyaite, $Na_2Si_{20}O_{40}(OH)_2 \cdot 8H_2O$. *J. Solid State Chem.* **2021**, *300*, 122215. [CrossRef]
28. Scott, M.; Auerbach, K.A.C.; Prabir, K.D. *Chapter 11: Alkali Silicates and Crystalline Silicic Acids*, 1st ed.; CRC Press: Boca Raton, FL, USA, 2004.
29. Fatima, H.; Seo, J.-D.; Kim, J.; Park, M. Adsorption Behavior of Kenyaite for Cu^{2+} and Pb^{2+}. *J. Porous Mater.* **2022**, *29*, 111–117. [CrossRef]
30. Ariyapala, K.D.S.D.; Withanage, W.I.U.; Takimoto, K.; Kumada, N.; Takei, T.; Saito, N.; Horikoshi, H. Ion-Exchange and Antibacterial Properties of Layered Silicate, Na-Kenyaite, Prepared Using Amorphous Silicon Dioxide (a-SiO_2) Blocks. *J. Ceram. Soc. Jpn.* **2024**, *132*, 39–44. [CrossRef]
31. Feng, F.; Balkus, K.J. Synthesis of Kenyaite, Magadiite and Octosilicate Using Poly(Ethylene Glycol) as a Template. *J. Porous Mater.* **2003**, *10*, 5–15. [CrossRef]
32. Fletcher, R.A.; Bibby, D.M. Synthesis of Kenyaite and Magadiite in the Presence of Various Anions. *Clays Clay Miner.* **1987**, *35*, 318–320. [CrossRef]
33. Kalvachev, Y.; Kostov-Kytin, V.; Todorova, S.; Tenchev, K.; Kadinov, G. Synthetic Kenyaite as Catalyst Support for Hydrocarbon Combustion. *Appl. Catal. B Environ.* **2006**, *66*, 192–197. [CrossRef]
34. Guerra, D.L.; Airoldi, C.; Viana, R.R. Adsorption of Arsenic(V) into Modified Lamellar Kenyaite. *J. Hazard. Mater.* **2009**, *163*, 1391–1396. [CrossRef] [PubMed]
35. Kooli, F.; Liu, Y.; Hbaieb, K.; Ching, O.Y.; Al-Faze, R. Characterization of Organo-Kenyaites: Thermal Stability and Their Effects on Eosin Removal Characteristics. *Clay Miner.* **2018**, *53*, 91–104. [CrossRef]
36. Kwon, O.Y.; Park, K.W. The Preparation of Flaky Layered Carbon by Using Layered Silicate Template. *Bull. Korean Chem. Soc.* **2003**, *24*, 1561–1562.
37. Oliveira, M.E.R.; da Silva Filho, E.C.; Filho, J.M.; Ferreira, S.S.; Oliveira, A.C.; Campos, A.F. Catalytic Performance of Kenyaite and Magadiite Lamellar Silicates for the Production of A,B-Unsaturated Esters. *Chem. Eng. J.* **2015**, *263*, 257–267. [CrossRef]
38. Royer, B.; Cardoso, N.F.; Lima, E.C.; Ruiz, V.S.O.; Macedo, T.R.; Airoldi, C. Organofunctionalized Kenyaite for Dye Removal from Aqueous Solution. *J. Colloid Interface Sci.* **2009**, *336*, 398–405. [CrossRef] [PubMed]
39. Sassi, M.; Miehé-Brendlé, J.; Patarin, J.; Bengueddach, A. Na-Magadiite Prepared in a Water/Alcohol Medium: Synthesis, Characterization and Use as a Host Material to Prepare Alkyltrimethylammonium- and Si-Pillared Derivates. *Clay Miner.* **2005**, *40*, 369–378. [CrossRef]
40. Kwon, O.Y.; Park, K.W.; Paek, U.H. Direct Synthesis of Na·Kenyaite from Amorphous Silica. *J. Korean Assoc. Cryst. Growth* **1999**, *9*, 70–73.
41. Sirinakorn, T.; Imwiset, K.; Bureekaew, S.; Ogawa, M. Inorganic Modification of Layered Silicates toward Functional Inorganic-Inorganic Hybrids. *Appl. Clay Sci.* **2018**, *153*, 187–197. [CrossRef]
42. Kooli, F.; Liu, Y.; Abboudi, M.; Oudghiri Hassani, H.; Rakass, S.; Ibrahim, S.M.; Al Wadaani, F. Waste Bricks Applied as Removal Agent of Basic Blue 41 from Aqueous Solutions: Base Treatment and Their Regeneration Efficiency. *Appl. Sci.* **2019**, *9*, 1237. [CrossRef]
43. Kebir, Z.A.M.; Adel, M.; Adjdir, M.; Bengueddach, A.; Sassi, M. Preparation and Antibacterial Activity of Silver Nanoparticles Intercalated Kenyaite Materials. *Mater. Res. Express* **2018**, *5*, 085021. [CrossRef]
44. Aicha, B.; Mohamed, S.; Jocelyne, M.-B.; Benedicte, L.; Jean-Luc, B.; Abdelkader, B. Preparation of New Microporous Titanium Pillared Kenyaite Materials Active for the Photodegradation of Methyl Orange. *J. Porous Mater.* **2018**, *25*, 801–812. [CrossRef]
45. Mochizuki, D.; Kuroda, K. Design of Silicate Nanostructures by Interlayer Alkoxysilylation of Layered Silicates (Magadiite and Kenyaite) and Subsequent Hydrolysis of Alkoxy Groups. *New J. Chem.* **2006**, *30*, 277–284. [CrossRef]
46. Huang, Y.; Jiang, Z.; Schwieger, W. Vibrational Spectroscopic Studies of Layered Silicates. *Chem. Mater.* **1999**, *11*, 1210–1217. [CrossRef]
47. Shtenberg, M.V.; Popov, V.A.; Lebedeva, S.M.; Zainullina, R.T.; Rassomakhin, M.A. Vibrational Spectroscopy of Kenyaite and Magadiite in the Southern Urals. In Proceedings of the Minerals: Structure, Properties, Methods of Investigation, Ekaterinburg, Russia, 5–8 February 2020; pp. 237–243.
48. Yang, J.; Zhu, J.; Zhang, S.; Lv, T.; Feng, Z.; Wang, Y.; Meng, C. Osda-Free Hydrothermal Conversion of Kenyaite into Zeolite Beta in the Presence of Seed Crystals. *Solid State Sci.* **2020**, *107*, 106370. [CrossRef]
49. Eypert-Blaison, C.; Humbert, B.; Michot, L.J.; Pelletier, M.; Sauzéat, E.; Villiéras, F. Structural Role of Hydration Water in Na- and H-Magadiite: A Spectroscopic Study. *Chem. Mater.* **2001**, *13*, 4439–4446. [CrossRef]
50. Jeong, S.-Y.; Suh, J.-K.; Jin, H.; Lee, J.-M.; Kwon, O.-Y. Preparation of Molecular Sieve from Pillaring of Kenyaite: Effects of Catalysts on Gellation of Intercalated Teos. *J. Colloid Interface Sci.* **1996**, *180*, 269–275. [CrossRef]
51. Borade, R.B.; Clearfield, A. Hydrothermal Synthesis of an Iron Silicate with Layered Structure. *Chem. Commun.* **1997**, *3*, 277–278. [CrossRef]
52. Crone, I.A.; Franklin, K.R.; Graham, P. A New Route for the Preparation of Hydrated Alkali-Metal Silicates. *J. Mater. Chem.* **1995**, *5*, 2007–2011. [CrossRef]
53. Bi, Y.; Lambert, J.-F.; Millot, Y.; Casale, S.; Blanchard, J.; Zeng, S.; Nie, H.; Li, D. Relevant Parameters for Obtaining High-Surface Area Materials by Delamination of Magadiite, a Layered Sodium Silicate. *J. Mater. Chem.* **2011**, *21*, 18403–18411. [CrossRef]

54. Koike, M.; Grosskreuz, I.; Asakura, Y.; Miyawaki, R.; Gies, H.; Wada, H.; Shimojima, A.; Marler, B.; Kuroda, K. Bridging the Gap between Zeolites and Dense Silica Polymorphs: Formation of All-Silica Zeolite with High Framework Density from Natural Layered Silicate Magadiite. *Chemistry* **2023**, *29*, e202301942. [CrossRef]
55. Abbas, M.; Harrache, Z.; Trari, M. Mass-Transfer Processes in the Adsorption of Crystal Violet by Activated Carbon Derived from Pomegranate Peels: Kinetics and Thermodynamic Studies. *J. Eng. Fibers Fabr.* **2020**, *15*, 1558925020919847. [CrossRef]
56. Abbas, M.; Trari, M. Mass Transfer Process in the Removal of Congo Red (Cr) onto Natural Clay (Nc): Kinetic, Isotherm Modeling, and Thermodynamic Study. *J. Water Clim. Change* **2023**, *14*, 2755–2772. [CrossRef]
57. Al Dmour, H.; Kooli, F.; Mohmoud, A.; Liu, Y.; Popoola, S.A. Al and Zr Porous Clay Heterostructures as Removal Agents of Basic Blue-41 Dye from an Artificially Polluted Solution: Regeneration Properties and Batch Design. *Materials* **2021**, *14*, 2528. [CrossRef] [PubMed]
58. Aziz, E.; Boutouil, A.; el Himri, M.; Rachid, L.; El Haddad, M. Selective and Competitive Removal of Three Basic Dyes from Single, Binary and Ternary Systems in Aqueous Solutions: A Combined Experimental and Theoretical Study. *J. Saudi Chem. Soc.* **2020**, *24*, 527–544. [CrossRef]
59. Mokhtar, M. Application of Synthetic Layered Sodium Silicate Magadiite Nanosheets for Environmental Remediation of Methylene Blue Dye in Water. *Materials* **2017**, *10*, 760. [CrossRef]
60. Swenson, H.; Stadie, N.P. Langmuir's Theory of Adsorption: A Centennial Review. *Langmuir* **2019**, *35*, 5409–5426. [CrossRef]
61. Roulia, M.; Vassiliadis, A.A. Interactions between C.I. Basic Blue 41 and Aluminosilicate Sorbents. *J. Colloid Interface Sci.* **2005**, *291*, 37–44. [CrossRef]
62. Baskar, A.V.; Bolan, N.; Hoang, S.A.; Sooriyakumar, P.; Kumar, M.; Singh, L.; Jasemizad, T.; Padhye, L.P.; Singh, G.; Vinu, A.; et al. Recovery, Regeneration and Sustainable Management of Spent Adsorbents from Wastewater Treatment Streams: A Review. *Sci. Total Environ.* **2022**, *822*, 153555. [CrossRef]
63. Şentürk, İ.; Alzein, M. Adsorptive Removal of Basic Blue 41 Using Pistachio Shell Adsorbent–Performance in Batch and Column System. *Sustain. Chem. Pharm.* **2020**, *16*, 100254. [CrossRef]
64. Alanazi, A.M.; Jefri, O.A.; Alam, M.G.; Al-Faze, R.; Kooli, F. Organo Acid-Activated Clays for Water Treatment as Removal Agent of Eosin-Y: Properties, Regeneration, and Single Batch Design Absorber. *Heliyon* **2024**, *10*, e30530. [CrossRef] [PubMed]